Supporting Information

Angerer et al. 10.1073/pnas.1322438111

SI Methods

Preparation of Intact Mitochondria. Cells grown in yeast-dextrose medium [2% (wt/vol) glucose, 0.5% yeast extract] were harvested at late exponential growth phase [optical density $(OD)_{600}$ ~10 OD] and washed with ice-cold washing buffer (10 mM Tris·Cl, 0.4 M mannitol, 1 mM EDTA, 0.05 mM EGTA at pH 7.2, + 4 mg/mL freshly added fatty acid-free BSA). The wet weight of the cells was determined, and the cells were then resuspended in 1 mL/g cells ice-cold disintegration buffer (10 mM Tris·Cl, 0.6 M mannitol, 0.05 mM EDTA, 1 mM EGTA at pH 7.2, + 4 mg/mL freshly added fatty acid-free BSA). Glass beads (0.5 mm, 1 g/g cells) were added, and the suspension was mixed for 10 min on ice, using a propeller type stirrer. Another portion of glass beads (0.25–0.5 mm, 0.5 g/g cells) was added, and stirring continued for 10 min on ice. Mitochondria were then prepared by differential centrifugation at 4 °C, using a JA20 rotor. The cells debris was removed by centrifugation at 3,000 rpm for 5 min, and the mitochondria were sedimented from the supernatant by centrifugation at 12,000 rpm for 10 min. The pellet was resuspended in ice-cold mitochondria washing buffer (10 mM Tris·Cl, 0.6 M mannitol, 0.05 mM EDTA, 0.05 mM EGTA at pH 7.2, + 4 mg/mL freshly added fatty acid-free BSA), and impurities were pelleted by centrifugation at 5,500 rpm for 5 min. The mitochondria-containing supernatant was again centrifuged for 10 min at 12,000 rpm. The sediment was resuspended in a small volume of mitochondria washing buffer and applied to sucrose step gradient centrifugation (rotor TH641, 27,000 rpm, 45 min, 4 °C). The mitochondria were collected and washed with EDTA-free buffer 10 mM Tris·Cl, 0.6 M mannitol at pH 7.2, + 1 mg/mL freshly added fatty acid-free BSA, and centrifuged again in rotor JA20 for 10 min at 12,000 rpm. After resuspending the pellet in EDTA-free buffer (~500 μL), the protein concentration was determined using a modified Lowry protocol subtracting the added 1 mg/mL BSA. Aliquots, 400 μg in size, of intact mitochondria (respiratory control ratio, ~5.8; state 3 vs. state 4 respiration) were frozen in liquid nitrogen.

Preparation of Mitochondrial Membranes and Purification and Fragmentation of Complex I. Mitochondrial membranes were prepared as described previously (1). Purification of n-dodecyl-β-D-maltoside solubilized complex I was carried out as detailed in ref. 1. The preparation of the peripheral arm fragment (Iλ) of *Yarrowia lipolytica* complex I was done essentially as described in ref. 2.

Electron Microscopy. Samples of the subcomplex *nb4m*Δ were diluted to ~15 μg/mL applied to continuous carbon-coated, glow-discharged grids and deep stain embedded in 2% phosphotungstic acid (pH 7.2). The sample was imaged at 100 kV under low-dose conditions. Images were recorded on a slow-scan CCD camera at a nominal magnification of 42,000, resulting in a calibrated pixel size of 3.02 Å. Images were recorded at a defocus of close to 1 μm, resulting in a resolution limit of ~2 nm within the first zero of the transfer function.

For image processing, a total of 6,559 images of single *nb4m*Δ particles were boxed out of the micrographs. In a first step, the images were interpolated down to a resolution of 3.6 Å for later comparison with the reference structure. As a reference, the contrast transfer function-corrected 0° images of the earlier random conical data set were used, which are the data used for the earlier 3D reconstruction of *Y. lipolytica* complex I (3). The sample for this reconstruction had also had been prepared by deep stain embedding in phosphotungstic acid.

The images of the subcomplex *nb4m*Δ were first centered against a rotationally symmetrized reference followed by rotational alignment toward two references that were two views of complex I from opposite sides, obtained from averages of the reference data set. In a second step, multireference alignment was carried out against the class averages obtained from the reference data set (3). The data set of the subcomplex contained predominantly one view and only a minority of images showing the complex in a flipped orientation. These flipped views were easily recognizable and were removed from the data, resulting in a final data set size of 5,202 images. The data set of the holocomplex had undergone prior classifications, in which process-flipped views had been removed (1), and contained 10,886 images. From the 5,202 aligned images of the subcomplex *nb4m*Δ, the average was calculated and subtracted from the total average of the holoenzyme data. For further analysis, both data sets were combined into a single image series, with the first 10,886 images being from the holocomplex and 5,202 images from the subcomplex *nb4m*Δ. The combined set was low-pass filtered to 30 Å and subjected to correspondence analysis. Of the 8 factors/principle components, factors 1, 2, and 4–8 were used for a classification using Diday's method of moving centers followed by hierarchical ascendant classification (4). Factor 3 was not included in the final classification, as this factor had the tendency to separate the two data sets. Because this information is known a priori, no new information could be gained by including this factor. A final number of seven classes was obtained. Each of the seven classes was split into two sets, with one containing the images of the subcomplex and the other containing only the images of the holocomplex. From both sets in each class, separate average images were calculated for comparison. The results clearly show that domain 6 is missing in each of the classes, confirming that the apparent lack of the domain is not a result of conformational variability.

Iron Determination. Iron-to-protein ratios were determined by total-reflection X-ray fluorescence, using a Picofox S2 spectrometer (Bruker) with MoKa radiation, and a measuring time of 1,000 s, essentially as described in ref. 5.

1. Kashani-Poor N, Kerscher S, Zickermann V, Brandt U (2001) Efficient large scale purification of his-tagged proton translocating NADH: Ubiquinone oxidoreductase (complex I) from the strictly aerobic yeast Yarrowia lipolytica. *Biochim Biophys Acta - Bioenerg* 1504:363–370.
2. Abdrakhmanova A, et al. (2004) Subunit composition of mitochondrial complex I from the yeast Yarrowia lipolytica. *Biochim Biophys Acta* 1658(1-2):148–156.
3. Radermacher M, et al. (2006) The three-dimensional structure of complex I from Yarrowia lipolytica: A highly dynamic enzyme. *J Struct Biol* 154(3):269–279.
4. Diday E (1971) La methode des nuees dynamiques. *Rev Stat Appl* 19:19–33.
5. Zickermann V, Wittershagen A, Kolbesen BO, Ludwig B (1997) Transformation of the CuA redox site in cytochrome c oxidase into a mononuclear copper center. *Biochem* 36:3232–3236.

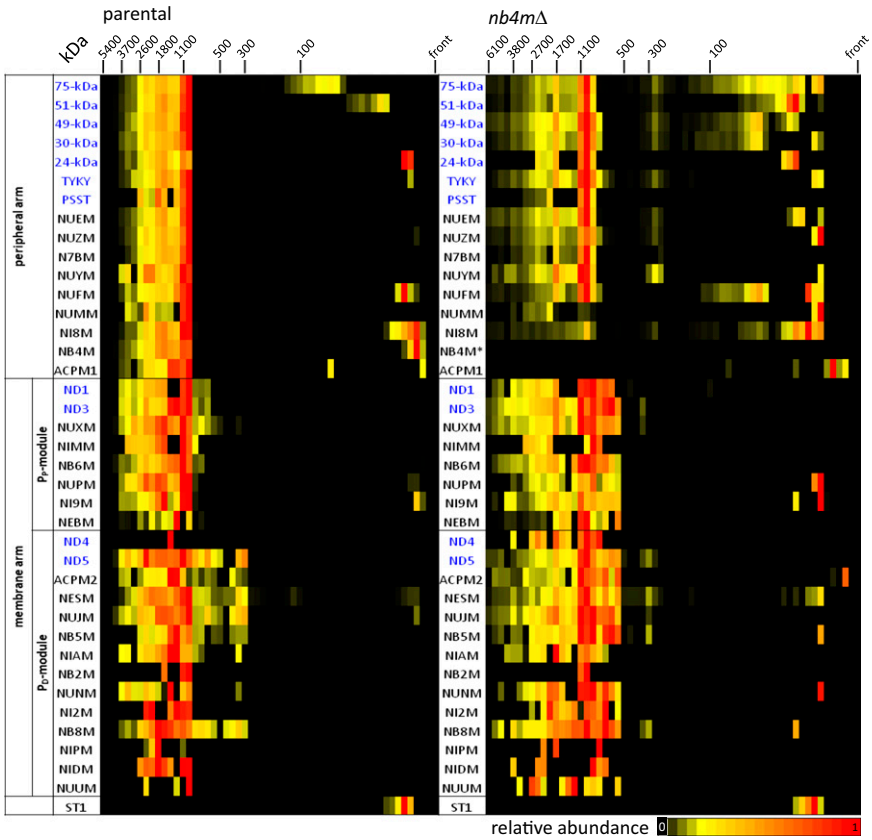

Fig. S1. Complexome Profiling of intact mitochondria of the parental strain and strain *nb4m*Δ. Migration profiles in heat map representation of the subunits of the peripheral and the membrane arm of complex I that were derived from complete Complexome Profiles of digitonin-solubilized intact mitochondria. *No peptides detected; see *Results* and Tables S1 and S2. P_D-module, distal pump module; P_P-module, proximal pump module.

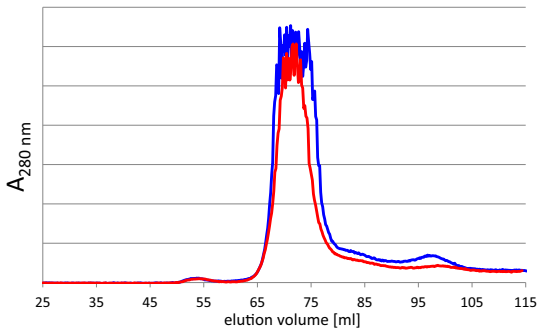

Fig. S2. Profile of size-exclusion chromatography. Purification of complex I from strain *nb4m*Δ (red) was straightforward, and the final gel filtration chromatography on a TSK 4000SW column did not resolve a difference in size with complex I from the parental strain (blue). The strong noise at the peak maximum reflects a signal overflow at the detector.

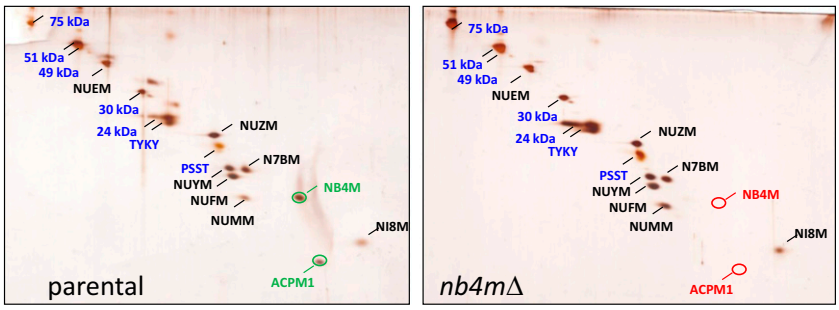

Fig. S3. Doubled (d) SDS-PAGE analysis of the peripheral arm fragment Iλ, generated from parental complex I and complex I from strain *nb4m*Δ. Protein complexes were disintegrated by exposure to the harsh detergent lauryldimethylamine-oxide and repurified. The subunit composition of the peripheral arm fragment Iλ was confirmed by mass spectrometry (Table S1). First dimension, 10% SDS/PAGE + 6 M urea; second dimension, 16% SDS/PAGE; blue captions, central subunits; black captions, accessory subunits; NB4M and mitochondrial acyl carrier protein subunit ACPM1 are highlighted in green; the corresponding position in the gel of the Iλ fragment of the deletion strain is indicated by red circles.

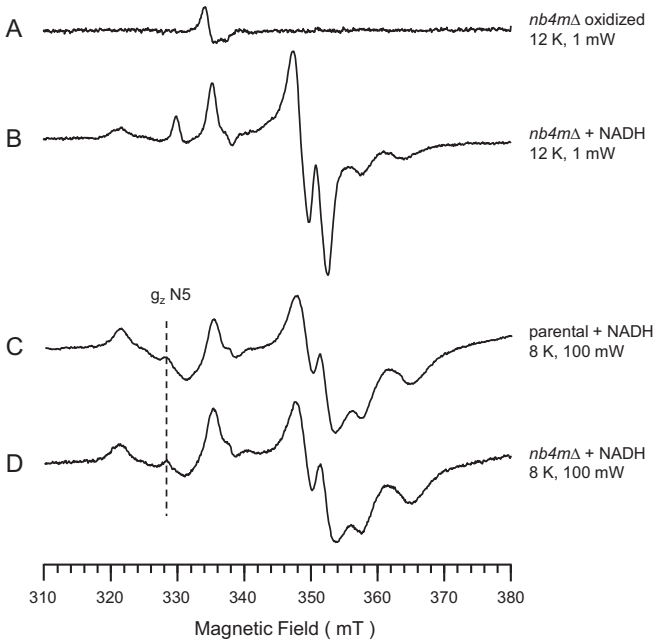

Fig. S4. Electron spin resonance (EPR) spectrum of purified complex I from strain *nb4m*Δ. At 12 K, complex I of the mutant in the oxidized state shows an EPR signal characteristic for 3Fe–4S clusters (*A*), but the signal intensity is low, as can be deduced from the EPR spectrum of the same sample reduced by nicotinamide adenine dinucleotide (reduced form) (NADH), which was recorded under identical conditions (*B*). The signal in the oxidized state most likely represents defective iron–sulfur cluster N2, but the intensity is far too low to account for the missing 40% in signal intensity, as estimated from double integration of the difference spectrum from Fig. 2 and the spectrum of the oxidized sample. At 8 K and high microwave power, iron–sulfur cluster N5 is detectable in mutant complex I without any changes compared with the parental sample (*C* and *D*).

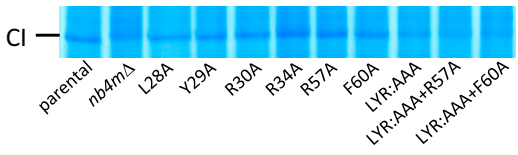

Fig. S5. Complex I content of mitochondrial membranes assessed by blue native (BN)-PAGE. Complex I band (CI) from BN-PAGE of dodecylmaltoside-solubilized mitochondrial membranes.

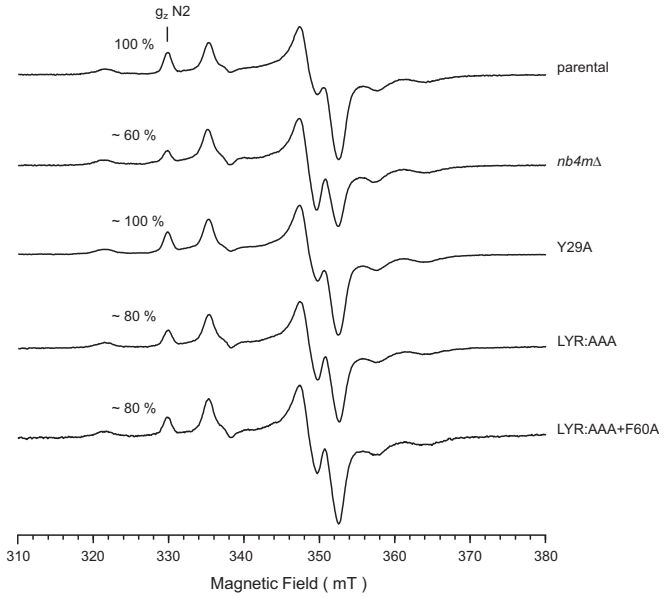

Fig. S6. EPR spectra recorded at 12 K of purified parental and mutant complex I reduced by NADH. The indicated relative intensities of N2 were obtained after normalization on the intensities of EPR signals N3 and N4 of the parental sample (see also Fig. 2) and comparison of the amplitudes of the g_z component of cluster N2 EPR signals in the parental sample with those of the mutant samples (see also Table 1).

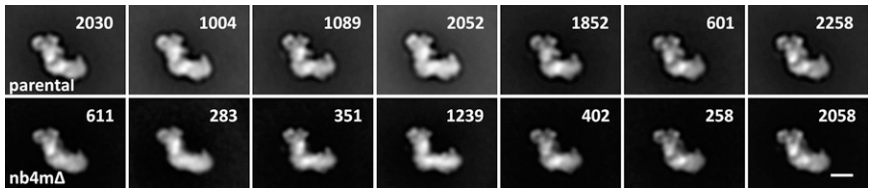

Fig. S7. Seven class averages obtained from a classification combined data set containing both the images of the holocomplex and the images of the subcomplex from strain *nb4m*Δ. (*Upper*) Class averages calculated only from the images of the parental complex I contained in each class. (*Lower*) Calculated only from the images from strain *nb4m*Δ contained in each class. The number of images contributing to each average is indicated. The comparison between the average images of the complete complex I and of the subcomplex clearly show that domain 6 is missing in the strain *nb4m*Δ in all class averages. All images are shown low-pass filtered to 3-nm resolution. (Scale bar, 10 nm.)

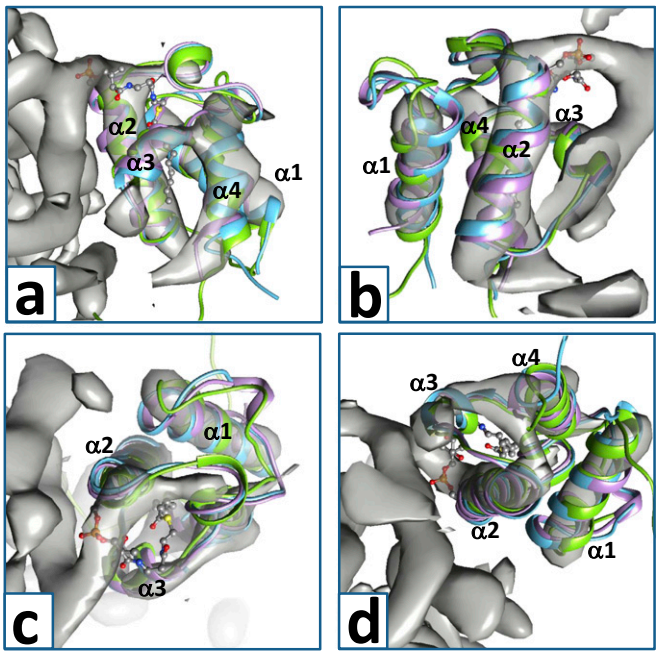

Fig. S8. Structural model of acyl carrier protein ACPM1 residing at the distal end of subdomain 6. Fit of structural model for subunit ACPM1 (cyan), one representative conformer of the NMR structure of the human mitochondrial acyl carrier protein NADH dehydrogenase (ubiquinone) Alpha/Beta subcomplex subunit 1 (NDUFAB1) (2DNW; green), and X-ray structure of ACP from *Escherichia coli* [2FAE (1), pink] into the X-ray electron density map of *Y. lipolytica* complex I (2) (gray, contour level 1.3, clipping adjusted for optimal visibility of acyl carrier protein). The characteristic acyl carrier protein fold comprises four helices (α1-α4); the decanoyl-phosphopantetheine bound to Serine-36 of the *E. coli* ACP is resolved (ball and stick representation, color element-specific); the position of the phosphate moiety coincides with a connectivity between the tip of helix α-2 of the acyl carrier protein and an adjacent helical feature in the electron density map assigned to subunit NB4M (see *Results*). (*A* and *B*) side views, (*C*) top view, (*D*) view from below into the central cavity accommodating the decanoyl-phosphopantetheine; for orientation in *A*, compare Fig. 5*B*.

1. Roujeinikova A, et al. (2007) Structural studies of fatty acyl-(acyl carrier protein) thioesters reveal a hydrophobic binding cavity that can expand to fit longer substrates. *J Mol Biol* 365(1): 135–145.
2. Hunte C, Zickermann V, Brandt U (2010) Functional modules and structural basis of conformational coupling in mitochondrial complex I. *Science* 329(5990):448–451.

Table S1. Subunit composition of parental complex I, complex I from strain nb4mΔ, and the corresponding Iλ fragments representing the peripheral arm

	Complex I*		Complex Iλ†	
Subunit	Parental	*nb4m*Δ	Parental	*nb4m*Δ
Peripheral arm				
75 kDa	115/2687	133/3039	76/1647	81/1740
51 kDa	81/2062	99/2322	53/1047	44/1099
49 kDa	127/1838	131/1951	53/920	59/1190
30 kDa	76/1453	86/1574	51/823	58/863
24 kDa	33/659	33/657	10/209	8/285
TYKY	31/811	31/730	24/534	18/417
PSST	19/350	21/345	10/211	7/215
NUEM	87/1450	96/1711	55/1042	46/1104
NUZM	30/684	42/720	33/543	42/543
N7BM	21/448	20/486	13/198	18/239
NUYM	26/507	32/531	20/243	23/218
NUFM	45/672	48/713	15/250	16/349
NUMM	14/403	17/429	7/215	7/208
NI8M	7/263	9/347	6/193	5/161
NB4M	26/390	—	19/281	—
ACPM1	9/270	—	4/139	—
Membrane arm				
ND1	2/30	2/73	—	—
ND2	—	—	—	—
ND3	10/245	9/226	—	—
ND4	9/227	8/265	—	—
ND5	24/571	24/588	—	—
ND6	—	—	—	—
ND4L	1/33	1/23	—	—
NESM	50/1180	54/1319	—	—
NUJM	25/441	33/546	—	3/75
NUPM	18/519	26/746	—	—
NUXM	26/561	40/538	—	—
NIAM	24/462	27/568	—	—
NB6M	17/416	18/431	—	—
NUNM	14/367	19/432	—	—
NI2M	12/359	14/368	—	—
NB8M	4/169	4/182	—	—
NB5M	8/94	6/107	—	—
ACPM2	6/134	8/172	—	—
NIPM	3/106	3/137	—	—
NIMM	16/370	19/310	—	—
NI9M	10/316	13/368	—	1/31
NB2M	9/268	17/286	—	—
NEBM	9/261	10/335	—	—
NUUM	9/305	9/308	—	—
NIDM	1/40	1/48	—	—
ST1	—	—	—	—

Number of MS/MS spectra that were matched to the protein/Mascot score. Mascot search parameters: peptide mass tolerance, 10 ppm; fragment mass tolerance, 0.8 kDa; maximum missed cleavage sites, 2; fixed modifications, carbamidomethyl (C); variable modification, oxidation (M); enzyme, trypsin; all peptides were filtered for significant hits (Mascot significance threshold $P < 0.05$; cut off, 16). Bold captions, central subunits; nonbold captions, accessory subunits.

*Blue native electrophoresis (BNE), band of affinity purified complex I.

†Prepared from purified complex I; BNE band of purified subcomplex Iλ.

Table S2. Complete protein identification data of the complexome profiles shown in Fig. S1

Subunit*	Remarks†	Parental‡	*nb4mΔ*‡
75 kDa	NUAM, YALI0D05467g, mature, 75.2 kDa	46.4% cov., 498 hits, 26 pep.	49.14% cov., 482 hits, 24 pep.
51 kDa	NUBM, YALI0B20372g, mature, 51.6 kDa	62.13% cov., 251 hits, 22 pep.	53.4% cov., 239 hits, 19 pep.
49 kDa	NUCM, YALI0F17248g, mature, 49.9 kDa	61.04% cov., 304 hits, 19 pep.	62.61% cov., 274 hits, 18 pep.
30 kDa	NUGM, YALI0F02123g, mature, 29.2 kDa	70.92% cov., 222 hits, 17 pep.	75.7% cov., 280 hits, 17 pep.
24 kDa	NUHM, YALI0D00737g, mature, 24.1 kDa	42.79% cov., 88 hits, 9 pep.	27.91% cov., 23 hits, 4 pep.
TYKY	NUIM, YALI0F00924g, mature, 22.3 kDa	67.17% cov., 117 hits, 9 pep.	60.61% cov., 151 hits, 7 pep.
PSST	NUKM, YALI0F06050g, mature, 20.4 kDa	54.1% cov., 20 hits, 5 pep.	42.62% cov., 15 hits, 3 pep.
NUEM	NUEM, YALI0D24585g, mature, 40.4 kDa	69.3% cov., 399 hits, 20 pep.	67.04% cov., 269 hits, 17 pep.
NUZM	NUZM, YALI0A02651g, 19.7 kDa	65.38% cov., 179 hits, 10 pep.	79.12% cov., 170 hits, 11 pep.
N7BM	N7BM, YALI0B00792g, 16.1 kDa	38.41% cov., 62 hits, 5 pep.	38.41% cov., 41 hits, 4 pep.
NUYM	NUYM, YALI0B14861g, mature, 15.9 kDa	62.04% cov., 57 hits, 6 pep.	47.45% cov., 69 hits, 5 pep.
NUFM	NUFM, YALI0E23089g| mature, 15.6 kDa	35.29% cov., 89 hits, 5 pep.	35.29% cov., 107 hits, 5 pep.
NUMM	NUMM,YALI0D19030g, 15.1 kDa	26.47% cov., 21 hits, 2 pep.	39.71% cov., 22 hits, 3 pep.
NI8M	NI8M, YALI0C03201g, 9.6 kDa	16.09% cov., 40 hits, 1 pep.	45.98% cov., 72 hits, 3 pep.
NB4M	NB4M, YALI0A01419g, mature,14.6 kDa	65.85% cov., 160 hits, 6 pep.	no peptides identified
ACPM1	ACPM1, YALI0D14850g, 12 kDa	37.61% cov., 61 hits, 4 pep.	43.12% cov., 53 hits, 5 pep.
ND1	NU1M, ND1, 38.3 kDa	2.35% cov., 23 hits, 1 pep.	2.35% cov., 19 hits, 1 pep.
ND3	NU3M, ND3, 14.5 kDa	21.88% cov., 38 hits, 2 pep.	21.88% cov., 33 hits, 2 pep.
NUXM	NUXM, YALI0E28424g, 18.6 kDa	31.36% cov., 111 hits, 5 pep.	31.36% cov., 131 hits, 5 pep.
NIMM	NIMM, YALI0C21789g, 9.8 kDa	31.03% cov., 18 hits, 3 pep.	31.03% cov., 12 hits, 3 pep.
NB6M	NB6M, YALI0E28930g, 14.1 kDa	41.46% cov., 81 hits, 4 pep.	41.46% cov., 79 hits, 4 pep.
NUPM	NUPM, YALI0A20680g, 19.3 kDa	61.05% cov., 80 hits, 8 pep.	73.26% cov., 95 hits, 11 pep.
NI9M	NI9M, YALI0E23749g, 9 kDa	55.13% cov., 35 hits, 3 pep.	56.41% cov., 66 hits, 4 pep.
NEBM	NEBM, 8 kDa	22.97% cov., 18 hits, 1 pep.	22.97% cov., 22 hits, 1 pep.
ND4	NU4M, ND4, 54.4 kDa	2.47% cov., 1 hits, 1 pep.	4.32% cov., 21 hits, 2 pep.
ND5	NU5M, ND5, 73.7 kDa	11.76% cov., 76 hits, 7 pep.	15.11% cov., 116 hits, 8 pep.
ACPM2	ACPM2, YALI0D24629g, 14.4 kDa	23.48% cov., 72 hits, 3 pep.	23.48% cov., 56 hits, 3 pep.
NESM	NESM, YALI0E29095g, mature, 23.4 kDa	61.76% cov., 383 hits, 14 pep.	53.43% cov., 278 hits, 10 pep.
NUJM	NUJM, YALI0E11891g, 20.8 kDa	27.27% cov., 83 hits, 4 pep.	36.87% cov., 97 hits, 5 pep.
NB5M	NB5M, YALI0F06061g, mature, 10.3 kDa	30.43% cov., 42 hits, 2 pep.	30.43% cov., 58 hits, 2 pep.
NIAM	NIAM, YALI0D04939g, mature, 14.6 kDa	47.2% cov., 87 hits, 5 pep.	43.2% cov., 42 hits, 4 pep.
NB2M	NB2M, YALI0D10274g, 6.9 kDa	16.67% cov., 3 hits, 1 pep.	51.67% cov., 4 hits, 2 pep.
NUNM	NUNM, YALI0F14003g, 15.8 kDa	41.73% cov., 28 hits, 5 pep.	41.73% cov., 55 hits, 6 pep.
NI2M	NI2M, YALI0D07216g, 12.9 kDa	28.44% cov., 16 hits, 3 pep.	25.69% cov., 19 hits, 3 pep.
NB8M	NB8M, YALI0E31766g, mature, 11.1 kDa	58.16% cov., 58 hits, 5 pep.	43.88% cov., 43 hits, 3 pep.
NIPM	NIPM, YALI0F18359g, 10 kDa	42.7% cov., 9 hits, 3 pep.	10.11% cov., 3 hits, 1 pep.
NIDM	NIDM, YALI0A17946g, 11 kDa	9.78% cov., 9 hits, 1 pep.	9.78% cov., 6 hits, 1 pep.
NUUM	NUUM, 9.8 kDa	31.11% cov., 3 hits, 2 pep.	31.11% cov., 13 hits, 2 pep.
ST1	ST1, YALI0F23551g, 34.6 kDa	40.63% cov., 30 hits, 8 pep.	48.57% cov., 17 hits, 10 pep.

*Bold captions, central subunits; nonbold captions, accessory subunits. Hydrophobic central subunits ND2, ND6, and ND4L were not identified.

†Swiss-prot identifier, accession number Genolevures data bank (1), protein mass, in case of cleavage of N-terminal methionine or signal sequence is known, the mass of the mature protein is indicated (2).

‡Coverage (cov.), hits, and unique peptides (pep).

1. Radermacher M, et al. (2006) The three-dimensional structure of complex I from Yarrowia lipolytica: A highly dynamic enzyme. *J Struct Biol* 154(3):269–279.
2. Diday E (1971) La methode des nuees dynamiques. *Rev Stat Appl* 19:19–33.